JOURNAL OF GUIDANCE, CONTROL, AND DYNAMICS
Vol. 30, No. 3, May–June 2007

Prediction of Icing Effects on the Dynamic Response of Light Airplanes

Amanda Lampton* and John Valasek†
Texas A&M University, College Station, Texas 77843-3141

DOI: 10.2514/1.25687

The accumulation of ice on an airplane in flight is one of the leading contributing factors to general aviation accidents. To date, only relatively sophisticated methods based on detailed empirical data and flight data exist for its analysis. This paper develops a methodology and simulation tool for preliminary safety and performance evaluations of airplane dynamic response and climb performance in icing conditions. The important aspect of dynamic response sensitivity to pilot control input with the autopilot disengaged is also highlighted. Using only basic mass properties, configuration, propulsion data, and known icing data from a similar configuration, icing effects are applied to the dynamics of a non-real-time, six degree-of-freedom simulation model of a different, but similar, light airplane. Besides evaluating various levels of icing severity, the paper addresses distributed icing which consists of wing alone, horizontal tail alone, and unequal distributions of combined wing and horizontal tail icing. Results presented in the paper for a series of simulated climb maneuvers with various levels and distributions of ice accretion show that the methodology captures the basic effects of ice accretion on pitch response and climb performance, and the sensitivity of the dynamic response to pilot control inputs.

Nomenclature

A	=	plant matrix
B	=	control distribution matrix
C	=	output matrix
$C_{(A)}$	=	arbitrary stability and control derivative
$C_{(A)_{\text{iced}}}$	=	arbitrary stability and control derivative with icing effects
C_D	=	airplane drag coefficient
C_L	=	airplane lift coefficient
C_m	=	airplane pitching moment coefficient
C_Z	=	stability z-axis coefficient

Amanda Lampton earned the B.S. Cum Laude with Distinction (2004) and M.S. in aerospace engineering (2006) from Texas A&M University as a participant in the Engineering Scholars Program. She is a recipient of the National Science Foundation Graduate Fellowship, the Zonta International Foundation Amelia Earhart Fellowship, the Armed Forces Communications and Electronics Assoc. (AFCEA) General John A. Wickham Scholarship, and the United States Academic Decathlon Scholarship. She is a member of Sigma Gamma Tau, the aerospace engineering honor society, Phi Kappa Phi, Tau Beta Pi, the National Society of Collegiate Scholars, Phi Eta Sigma, the Society of Women Engineers, and the Texas A&M University Sky Diving Club, and Cycling Team. In 2005, she interned at Eclipse Aviation, performing parameter identification and aerodynamic data reduction with the Eclipse 500 flight test group. She is currently a graduate research assistant and Ph.D. candidate in the Flight Simulation Laboratory at Texas A&M University, researching ice accretion effects on aircraft dynamics and stability, and artificial intelligence techniques for control of morphing air vehicles. She is a member of AIAA.

John Valasek earned the B.S. degree in aerospace engineering from California State Polytechnic University, Pomona in 1986, and the M.S. degree with honors, and the Ph.D. in aerospace engineering from the University of Kansas, in 1991 and 1995, respectively. He was a flight control engineer for the Northrop Corporation, Aircraft Division from 1985 to 1988, where he worked in the Flight Controls Research Group, and on the AGM-137 Tri-Services Standoff Attack Missile (TSSAM) program. He previously held an academic appointment at Western Michigan University (1995-1997), was a summer faculty researcher at NASA Langley Research Center (1996), and an Air Force Office of Scientific Research (AFOSR) summer faculty research fellow at the Air Force Research Laboratory (1997). Since then, he has been with Texas A&M University, where he is Associate Professor of aerospace engineering, and Director of the Flight Simulation Laboratory. He teaches courses on digital control, nonlinear systems, flight mechanics, aircraft design, and coteaches a short course on digital flight control for the University of Kansas Division of Continuing Education. Current research interests include control of morphing air and space vehicles, multi-agent systems, intelligent autonomous control, vision-based navigation systems, and fault-tolerant adaptive control. He is an Associate Fellow of AIAA, past Chairman and current member of the Atmospheric Flight Mechanics Technical Committee, and current member of the Intelligent Systems, Guidance Navigation, and Control Technical Committees.

Presented as Paper 6219 at the Atmospheric Flight Mechanics, San Francisco, CA, 15–18 August 2005; received 16 June 2006; accepted for publication 27 November 2006.

*Graduate Research Assistant, Flight Simulation Laboratory, Aerospace Engineering Department, 3141 TAMU; alampton@tamu.edu. Student Member AIAA.
†Associate Professor and Director, Flight Simulation Laboratory, Aerospace Engineering Department, 3141 TAMU; valasek@tamu.edu. Associate Fellow AIAA.

$\bar{c}$ = mean geometric chord
D = carry through matrix
f_{ice} = icing factor
g = gravitational acceleration
h = integration step size
I_{yy} = airplane moment of inertia about y axis
i = index, imaginary component
j = imaginary component
k'_{C_A} = coefficient icing factor constant
L = roll angular acceleration
M = pitch angular acceleration; modal matrix
N = yaw angular acceleration
$n$frames = number of time steps
P = airplane body-axis roll rate
p = perturbed airplane body-axis roll rate
Q = airplane body-axis pitch rate
q = perturbed airplane body-axis pitch rate
$\dot{q}$ = airplane body-axis pitch acceleration
$\bar{q}$ = dynamic pressure
R = airplane body-axis yaw rate
r = perturbed airplane body-axis yaw rate
S = wing area
t = time
U = airplane velocity in the body-axis x direction
$\boldsymbol{U}$ = control input vector
u = stability axis airplane velocity in the x direction
$\dot{u}$ = incremental change in the stability axis airplane velocity in the x direction
V = airplane velocity in the body-axis y direction
W = airplane velocity in the body-axis z direction
$\dot{w}$ = incremental change in the stability axis airplane velocity in the z direction
X = linear acceleration in the body x-axis direction
$\boldsymbol{X}$ = state vector
$\dot{\boldsymbol{X}}$ = derivative of state vector
Y = linear acceleration in the body y-axis direction
$\boldsymbol{Y}$ = output vector
Z = linear acceleration in the body z-axis direction
α = angle of attack
$\dot{\alpha}$ = incremental change in angle of attack
Γ = discrete control distribution matrix
δ = control deflection angle
ζ = damping ratio
η_{ice} = icing severity parameter
Θ_1 = airplane steady-state pitch attitude angle
θ = pitch attitude angle
$\dot{\theta}$ = incremental change in pitch attitude angle
ν = eigenvector
ξ = modal vector
τ = time constant; dummy time variable
Φ = airplane roll attitude angle; discrete plant matrix
ω = frequency

Subscripts

a = aileron
d = Dutch roll mode
e = elevator
ice = ice accretion effect
iced = ice accretion effect
k = index for discretized model
m = modal
p = phugoid mode
q = derivative with respect to airplane pitch rate
r = rudder; roll mode
s = spiral mode
sp = short period mode
T_u = derivative with respect to change in speed due to thrust
T_α = derivative with respect to change in angle of attack due to thrust
u = derivative with respect to stability x-axis airplane velocity
α = derivative with respect to angle of attack
$\dot{\alpha}$ = derivative with respect to incremental change in angle of attack
δ_e = derivative with respect to elevator deflection angle
0 = derivative with respect to zero angle of attack; initial condition
1 = steady state; first mode
2 = second mode

I. Introduction

INCLEMENT weather accounted for an average of 19.6% of environment-related, reported general aviation accidents annually from 1998 to 2000 according to the National Transportation Safety Board [1–3]. Of this annual percentage, icing conditions accounted for 2.9% of general aviation accidents in 1997, 2.4% in 1998, 3.6% in 1999, and 2.7% in 2000, in which 36.4, 55.6, 46.2, and 40.0% of those resulted in fatalities in 1997, 1998, 1999, and 2000, respectively [1–4]. Rime, glaze, and mixed ice along the leading edge of lifting surfaces all have detrimental effects on airplane performance. Although anti-icing devices such as de-icing boots and heating strips help, ice accretions can still build up and affect the airplane adversely by increasing drag, decreasing airplane lift curve slope, and decreasing static longitudinal stability. Additionally, malfunctions of these anti-icing systems can result in ice buildup aft of the devices themselves, or ice buildup between the cycles of the de-icing systems. The type and severity of ice accretions is highly dependent on a number of factors. These include, but are not limited to, the following: velocity of the airplane, exposure time, atmospheric air temperature, liquid water content, and median volumetric diameter.

The danger of a climb with ice accretions on the airplane lays in the susceptibility of the ice to cause a separation bubble (Fig. 1) [5]. This phenomenon is usually caused by a horn of ice disrupting the flow of air over the airfoil and creating an adverse pressure gradient. This disruption forms a separation bubble that reattaches further downstream. However, increasing the elevator deflection angle also increases the angle of attack, thus pushing the reattachment point farther downstream and increasing the size of the separation bubble. As the bubble increases in size, elevator effectiveness decreases and full departure of the airplane becomes more likely. Bragg et al. have developed an icing-effects model applicable to any individual performance, stability, or control derivative affected by icing [6]. The model is characterized by dependence on atmospheric conditions, susceptibility of an airplane to icing, and a given derivative as seen in Eq. (1).

$$C_{(A)_{\text{iced}}} = (1 + \eta_{\text{ice}} k'_{C_A}) C_{(A)} \tag{1}$$

This model is still being refined, with many of the influencing factors still unknown [6]. The model was then integrated into a flight dynamics and control toolbox for MATLAB and Simulink [7], which produces results showing the possible changes of an airplane's stability derivatives over time with icing effects.

The practicality of using an autopilot during icing conditions has also been studied. Sharma et al. has designed a pitch angle hold autopilot that considers ice accretion severity when processing the

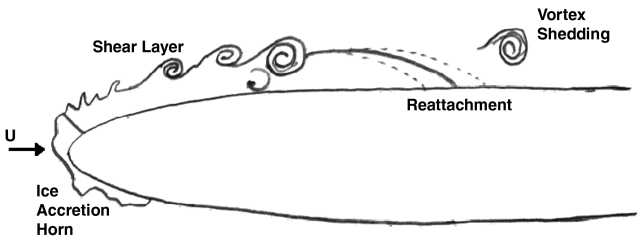

Fig. 1 Schematic of upper surface separation bubble aft of leading-edge ice accretion [5].

commanded pitch attitude angle; the goal being to maintain the stability of the airplane [8]. The commanded value for the pitch attitude angle is then modified based on an envelope protection algorithm that references flight test data of ice severity and wing stall angle of attack [8]. The purpose is to prevent the airplane from reaching the icing-modified wing stall angle of attack, and pitch attitude response is investigated. Distributed levels and severities of icing between the wing and horizontal tail are not specifically addressed, and the iced airplane model and the autopilot are applicable only to the DeHavilland Twin Otter [8]. Additionally, the important aspect of sensitivity of airplane response to pilot command inputs in icing conditions with the autopilot disabled, which is the autopilot status recommended by the Federal Aviation Administration (FAA) in these conditions, is not addressed.

The area of forensic engineering is also concerned with the effect ice has on climb performance and aerodynamic degradation [9]. The research described in [9] concerns the dangerous reduction in stall angle of attack and how climbing at high angles of attack could approach this reduced stall angle causing an unexpected wing stall. The nonlinear simulation incorporating the effects of ice accretion was set up specifically for a jet trainer in an attempt to project the trajectory of a crash caused by ice accretion [9].

Much other research in the area of the influence of ice regards airfoil aerodynamics. Lee and Bragg explore the changes in airfoil section lift, drag, and pitching moment with simulated ice shapes [10]. Intercycle ice accretions have a distinct effect on airfoil properties as described in [11]. In this case, the buildup of ice between pneumatic boot inflation and the possible ice ridge left just behind where the boot meets the skin of the airfoil is analyzed [11]. The resulting increase in drag, decrease in lift, and change in pitching moment is tabulated [11]. In general, the consensus appears to be that the aerodynamics of an airfoil is degraded by ice accretion such that lift decreases, drag increases, stall angle of attack is reduced, and pitching moment is degraded [9–16].

Efforts have been made to develop icing protection systems, especially by Bragg et al. [17]. They propose a smart icing system based on the ability to sense the effect of ice on aircraft performance, stability, and control. The system would enhance the level of safety offered by current icing avoidance and protection concepts [17]. The Smart Icing System senses ice accretion through traditional icing sensors and uses modern system identification methods to estimate aircraft performance and control changes [18].

Airplane response due to pilot command inputs with the autopilot disengaged is a critical safety issue, because the FAA recommends that the autopilot must be disengaged during flight in known icing conditions. The danger lies in a pilot attempting to command an iced airplane in the same way as a noniced airplane because overly aggressive pilot command inputs (for the iced situation) can produce excessive climb rates which can lead to stall, and/or overshoots and undershoots in commanded altitude. This is particularly critical for situations in which the pilot is not even aware that the airplane response and performance has been compromised by icing, and it has not been reported on in the open literature.

This paper details the development of a simplified method for the prediction of icing effects and pilot command effects on the dynamic response and climb performance of light airplanes, for which icing data may not exist or might not be obtainable. The method permits a rapid, first cut prediction and analysis of performance of icing effects using only basic, relatively easy to obtain or generate data as a precursor to a highly detailed analysis using sophisticated and costly modeling and analysis methods. It is equally applicable to either performance prediction or accident reconstruction and has been used for both. The unique contributions of this paper to the literature are threefold. It details a method to model and investigate airplanes for which icing data does not exist, or is not available in the open literature. This is done using known icing data obtained from either flight data or wind-tunnel data or both, for airplanes of similar but different configurations, using appropriate scaling and modification. It also considers the modeling and evaluation of unequally distributed icing levels and icing severity between the wing, the horizontal tail, and the full aircraft, in terms of dynamic response.

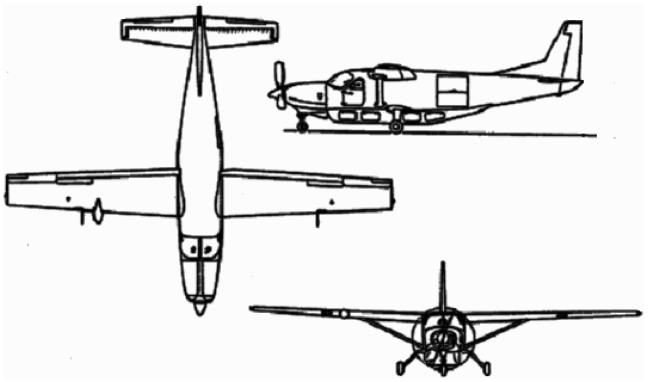

Fig. 2 Cessna 208B Super Cargomaster external characteristics [21].

The metrics used are rate-of-climb and commanded altitude captures consisting of overshoots and undershoots. Finally, this paper investigates sensitivity to pilot command inputs during icing conditions in terms of dynamic response and climb performance, with the autopilot disengaged as per FAA recommendation. The approach developed here is used to construct a linear time invariant (LTI), six degree of freedom, non-real-time flight simulation code which has the capability to evaluate a variety of time-varying pilot inputs, such as singlets, doublets, and ramps, during icing conditions. The scope of this work is limited to the pitch axis, where the most detrimental icing effects are typically experienced.

The paper is organized as follows. First, a nonparametric linear model of a Cessna 208B Super Cargomaster (Fig. 2) is developed, in which stability and control derivatives are calculated using data compendium (DATCOM) methods and the Advanced Aircraft Analysis (AAA) computer program [19]. Verification of the model is accomplished by comparing simulation data to published flight test data. To ensure the fidelity of the model, a modal analysis was conducted to examine the characteristics of the flight modes. In addition, a controllability analysis was conducted to check that the system was indeed linearly independent and controllable. Next, the stability derivatives calculated for each flight condition of interest are used to construct multiple LTI state-space models. Various levels of ice accretion severity are then added to the clean airplane simulation based on icing data gathered by NASA John H. Glenn Research Center on the DeHavilland Twin Otter [6]. A series of simulation examples are presented for climb maneuvers with varying amounts of ice accretion, together with an investigation of the dynamic effect of overcontrolling the airplane during a climb. Finally, a summary and conclusions are presented.

II. State-Space Model Representation

To determine the response of an LTI system to an arbitrary input signal, it is transformed into a state-space representation of the system. The system analyzed in this paper is a continuous dynamic linear system in the stability axis. Figure 3 shows the body-axis systems for reference. Time invariance of the model is assumed because the parameters in the model do not change quickly for the

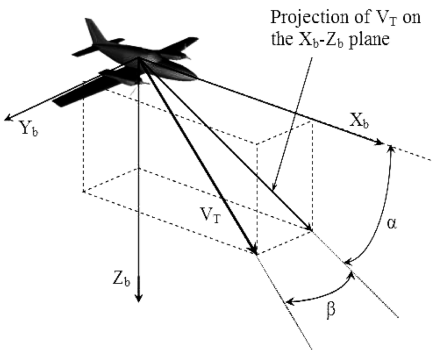

Fig. 3 Body-axis systems and aerodynamic angles.

relatively slow maneuvers examined here. Consider first the LTI state-space model of perturbations about the steady-state or trim condition

$$\dot{\boldsymbol{X}} = A\boldsymbol{X} + B\boldsymbol{U} \qquad \boldsymbol{Y} = C\boldsymbol{X} + D\boldsymbol{U} \tag{2}$$

where $\boldsymbol{X} \in \mathbb{R}^{n\times 1}$, $A \in \mathbb{R}^{n\times n}$, $\boldsymbol{U} \in \mathbb{R}^{m\times 1}$, $B \in \mathbb{R}^{n\times m}$, $\boldsymbol{Y} \in \mathbb{R}^{r\times 1}$, $C \in \mathbb{R}^{r\times n}$, and $D \in \mathbb{R}^{r\times m}$. Considering the longitudinal dynamics of an airplane, the linear equations of motion of this coupled system in stability axes are defined as Taylor series expansions:

$$\begin{aligned}
\dot{u} &= -g\cos\Theta_1\theta + (X_{T_u} + X_u)u + X_\alpha\alpha + X_q q \\
&\quad + X_{\delta_e}\delta_e + X_{\delta_T}\delta_T + X_{\dot{\alpha}}\dot{\alpha} \\
\dot{\alpha} &= \frac{\dot{w}}{U_1} = (-g\sin\Theta_1\theta + Z_u u + Z_\alpha\alpha + Z_q q + U_1 q \\
&\quad + Z_{\delta_e}\delta_e + Z_{\delta_T}\delta_T + Z_{\dot{\alpha}}\dot{\alpha})/U_1 \\
\dot{q} &= (M_{T_u} + M_u)u + (M_{T_\alpha} + M_\alpha)\alpha + M_q q + M_{\delta_e}\delta_e \\
&\quad + M_{\delta_T}\delta_T + M_{\dot{\alpha}}\dot{\alpha} \\
\dot{\theta} &= q
\end{aligned} \tag{3}$$

These affine in control, coupled equations assume steady, level 1 g trimmed flight in the stability axis system such that $P_1 = Q_1 = R_1 = V_1 = W_1 = \Phi_1 = 0$, and $\Theta_1 =$ constant. These equations can be decoupled by premultiplying by the mass matrix E:

$$E = \begin{bmatrix} 1 & -X_{\dot{\alpha}} & 0 & 0 \\ 0 & 1 - \frac{Z_{\dot{\alpha}}}{U_1} & 0 & 0 \\ 0 & -M_{\dot{\alpha}} & 1 & 0 \\ 0 & 0 & 0 & 1 \end{bmatrix} \tag{4}$$

such that

$$E\dot{\boldsymbol{X}} = A\boldsymbol{X} + B\boldsymbol{U} \Rightarrow \dot{\boldsymbol{X}} = E^{-1}A\boldsymbol{X} + E^{-1}B\boldsymbol{U} \tag{5}$$

where the state coefficient or plant matrix is now transformed into the decoupled form

$$E^{-1}A = \begin{bmatrix} X'_u & X'_\alpha & X'_q & X'_\theta \\ Z'_u & Z'_\alpha & Z'_q & Z'_\theta \\ M'_u & M'_\alpha & M'_q & M'_\theta \\ 0 & 0 & 1 & 0 \end{bmatrix} \tag{6}$$

in which the primed quantities result from collecting the $\dot{\alpha}$ terms in the lift equation, and eliminating the $\dot{\alpha}$ terms from the pitching moment equation. The corresponding control distribution matrix $B \in \mathbb{R}^{n\times m}$ is now represented by

$$E^{-1}B = \begin{bmatrix} X'_{\delta_e} & X'_{\delta_T} \\ Z'_{\delta_e} & Z'_{\delta_T} \\ M'_{\delta_e} & M'_{\delta_T} \\ 0 & 0 \end{bmatrix} \tag{7}$$

where the primes result for the same reason just given. The state and control vectors are represented by

$$\boldsymbol{X} = \begin{bmatrix} u & \alpha & q & \theta \end{bmatrix}^T \tag{8}$$

$$\boldsymbol{U} = \begin{bmatrix} \delta_e \\ \delta_T \end{bmatrix} \tag{9}$$

Assembling Eqs. (6–9) results in the model

$$\begin{bmatrix} \dot{u} \\ \dot{\alpha} \\ \dot{q} \\ \dot{\theta} \end{bmatrix} = \begin{bmatrix} X'_u & X'_\alpha & X'_q & X'_\theta \\ X'_u & X'_\alpha & X'_q & X'_\theta \\ X'_u & X'_\alpha & X'_q & X'_\theta \\ 0 & 0 & 1 & 0 \end{bmatrix} \begin{bmatrix} u \\ \alpha \\ q \\ \theta \end{bmatrix} + \begin{bmatrix} X'_{\delta_e} & X'_{\delta_T} \\ Z'_{\delta_e} & Z'_{\delta_T} \\ M'_{\delta_e} & M'_{\delta_T} \\ 0 & 0 \end{bmatrix} \begin{bmatrix} \delta_e \\ \delta_T \end{bmatrix} \tag{10}$$

The elements of Eqs. (6) and (7) are determined from nondimensional stability and control derivatives extracted from AAA for a DATCOM model of the Cessna 208B developed using the maintenance manual for the airplane [20] and verified by flight test data as shown in [21]. AAA is a code based on the U.S.Air Force Data Compendium (DATCOM). Major assumptions made in the development of the DATCOM model were 1) the exact location of the transition point from laminar to turbulent flow on the lifting surfaces, 2) the drag increment due to gaps between lifting and control surfaces, 3) steady flow, and 4) linear model is accurate up to angular displacements of 15 deg and velocity perturbations up to 100 ft/s. A universal location of 14% of the chord of the lifting surface is used as the transition point from laminar to turbulent flow. For the drag increment, a value of 0.00036 is used. Values of the stability and control derivatives used for calculations in this paper are provided in the Appendix.

Reference [21] contains the detailed modal analysis which is summarized here. The longitudinal dynamics consist of the two standard modes, short period and phugoid. Both are stable for the present flight condition.

Short period mode

$$\lambda_{1,2} = -1.49 \pm 2.54j \qquad \omega_{\text{sp}} = 2.94 \text{ rad/s} \qquad \zeta_{\text{sp}} = 0.51 \tag{11}$$

Phugoid mode

$$\lambda_{3,4} = -0.013 \pm 0.19j \qquad \omega_p = 0.2 \text{ rad/s} \qquad \zeta_p = 0.065 \tag{12}$$

A modal analysis was conducted to indicate contributions of each state and, in particular, each control, to the various longitudinal modes. For the Cessna 208B, the elevator is most effective in controlling pitch attitude angle and, to a lesser extent, angle of attack. In terms of modes, the first second-order mode is made up primarily of angle of attack and, to a lesser extent, pitch rate. The other second-order mode is mainly composed of pitch attitude angle and, to a lesser extent, angle of attack and pitch rate. The composition of these two modes indicates the existence of the standard short period and phugoid modes. A controllability analysis using the controllability gramian verifies that the system is controllable.

III. Simulation Development

Consistent with the scope of this work, which is to determine degradation due to ice accretions for several parameters via numerical simulation, the preceding continuous-time LTI model developed must be discretized. This discrete-time LTI system is defined as

$$\boldsymbol{X}_{k+1} = \Phi\boldsymbol{X}_k + \Gamma\boldsymbol{U}_k \qquad \boldsymbol{Y}_k = C\boldsymbol{X}_k + D\boldsymbol{U}_k \tag{13}$$

where $\Phi \in R^{n\times n}$ and $\Gamma \in R^{n\times m}$ are the state transition matrix and discrete control distribution matrix, respectively, and are dependent on the continuous $A \in R^{n\times n}$, $B \in R^{n\times m}$, and h, the time step of the discrete-time model. The Φ and Γ of the discrete model are computed from their continuous model counterparts, A and B, by the following equations:

$$\Phi = e^{Ah} \tag{14}$$

$$\Gamma = \left(\int_0^h e^{A\tau}\,\mathrm{d}\tau\right)B \tag{15}$$

The simulation is coded using MATLAB 7.0. By loading values determined from AAA for a given flight condition into the LTI state-space model in MATLAB, the discretized model can be determined using commands imbedded in the program. This is done for both a clean airplane and an iced airplane.

A thrust model was developed for the Cessna 208 Super Cargomaster based on the original manufacturer's model, which was stripped down into a FORTRAN source code, and converted into a linear MATLAB version. The purpose of this change was to

streamline the simulation as a whole, allowing thrust data to be updated every time step. This MATLAB-based thrust model was implemented and current data for the simulation was obtained using a series of table lookups in which the inputs are values such as current airspeed, rate of climb, ambient temperature, pressure, density, current altitude, and dynamic pressure. In addition, the thrust model is dependent on the prop control lever and power level position, which allows the throttle and therefore the thrust to be modified during the simulation. An example of this feature is shown later in this paper. The thrust model also accounts for corrections due to cabin heat, cabin temperature, and the status of the inertial separator system (ISS) in an effort to make the model as accurate as possible.

The thrust model calculations begin with determining inlet temperature and pressure. Then it proceeds to calculate fuel flow and gas generator speeds based on the settings for the ISS, power lever angle, and power control lever. Additional corrections were introduced to take into account decreases in fuel flow and gas generator revolutions per minute losses due to the ISS, cabin heat, and high-powered climbs. Propeller revolutions per minute are then determined using the values already calculated. Finally, shaft horsepower, net propeller thrust, gross jet thrust, ram drag, prop efficiency, air flow, and airplane thrust coefficient are calculated with corrections for the ISS and cabin heat. These data are used to determine the control derivatives due to thrust, as well as thrust and drag due to thrust for each time step of the simulations.

IV. Modeling and Incorporation of Icing Effects

The extent to which each stability and control derivative is affected by ice accretions is based on previous studies, in particular those concerning the flight dynamics of a DeHavilland Twin Otter [6,22]. Twin Otter data were used because there is more icing data available of the type needed for this research than for any other airplane reported in the open literature. In general, the effectiveness of C_L, C_m, C_D, C_{L_α}, C_{m_α}, C_{D_α}, C_{L_q}, C_{m_q}, $C_{L_{\delta_e}}$, and $C_{m_{\delta_e}}$ have been observed to degrade between 5 and 35%. As ice builds up on the leading edge of the wing and horizontal tail, the carefully engineered lifting surfaces are compromised, thus they produce less lift. Also, the ice accretion may develop horns that protrude into the airflow as well as increasing surface roughness leading to an increase in drag. The exact amount of degradation, whether it is an increase in lift, decrease in drag, or change in pitching moment, depends on both the airplane configuration and the particular derivative in question. The percentage of degradation for each derivative is imbedded within the MATLAB program that dimensionalizes the values calculated by AAA. Each of these dimensionalized counterparts of the derivatives is multiplied by an icing factor causing the derivative in question to become less stable. For example, the modification for C_{m_α} is

$$M_{\alpha_{\text{iced}}} = \frac{\bar{q}S\bar{c}^*(1 + f_{\text{ice}})^* C_{m_\alpha}}{Iyy} \tag{16}$$

such that static stability is reduced as C_{m_α} decreases. In this case, an f_{ice} value of -0.099 is the degradation factor, meaning that C_{m_α} becomes less stable by almost 10%, based on data from the DeHavilland Twin Otter [6]. For the numerical examples, these degradation factors are assumed to be the worst case scenario for icing on the Cessna 208B.

Equation (16) generalizes the terms first presented in Eq. (1). For the purposes of this research, f_{ice} represents the term $\eta_{\text{ice}} k'_{C_A}$. The actual parameterization of the terms η_{ice} and k'_{C_A} is beyond the scope of this paper, but is being addressed by other researchers. Instead, f_{ice} for each pertinent longitudinal derivative is calculated from flight test data of the DeHavilland Twin Otter in both clear and icing conditions, as detailed in [6]. Because comprehensive icing data are not readily available for the Cessna 208B, applying icing data obtained from the DeHavilland Twin Otter does not fully represent what actually occurs in icing conditions. However, the simulated dynamic responses and performance are consistent with the limited scope and objectives of this research. Values of f_{ice} are presented in Table 1.

Table 1 Change in stability and control derivatives (f_{ice}) due to icing [6]

Derivative	Definition	f_{ice}
ΔC_{Z_0}	$-\Delta C_{L_0}$	0
ΔC_{Z_A}	$-\Delta C_{L_\alpha} - \Delta C_{D_1}$	−0.10
ΔC_{Z_q}	$-\Delta C_{L_q}$	−0.014
$\Delta C_{Z_{\delta e}}$	$-\Delta C_{L_{\delta e}}$	−0.095
ΔC_{m_0}	ΔC_{m_0}	0
ΔC_{m_α}	ΔC_{m_α}	−0.099
ΔC_{m_q}	ΔC_{m_q}	−0.035
$\Delta C_{m_{\delta e}}$	$\Delta C_{m_{\delta e}}$	−0.10

To analyze how the flight dynamics and performance change with ice accretion severity, additional factors are included in the calculation of the iced derivatives to represent various levels of severity. For example, the nominal f_{ice} degradation factor for C_{m_α} is −0.099, as stated before. For a totally iced condition, the worst case for the Cessna 208B is f_{ice} multiplied by 1.0. It is assumed that the 1.0 is implicit in Eq. (16). Similarly, if only mild icing is of interest, then f_{ice} may only be multiplied by 0.2, as shown in the following equation

$$M_{\alpha_{\text{iced}}} = \frac{\bar{q}S\bar{c}(1 + 0.2f_{\text{ice}})C_{m_\alpha}}{Iyy} \tag{17}$$

For the example shown, $0.2f_{\text{ice}} = 0.2(-.099) = -0.0198$, which means that for "mild" ice C_{m_α} becomes less stable by about 2%. This additional severity factor allows for increased versatility in examining possible effects icing has on the flight dynamics and performance of the airplane in question.

Predicting the extent and severity of ice accretion before encountering icing conditions can be difficult due to its dependence on the configuration of the airplane and numerous atmospheric conditions: an airplane may be easily affected by even the smallest amount of ice, or it may be able to stay in flight without any adverse effects with very severe icing. In addition, an airplane does not necessarily have to accumulate ice evenly between lifting surfaces. Some airplanes tend to have a wing-icing problem only, others a horizontal-tail-icing problem, and still others do in fact accumulate ice fairly evenly between lifting surfaces. It is assumed here that the effects of distributed icing (different levels of ice on the wing and horizontal tail) appear as changes in the lift force and drag force of a given lifting surface, such as a wing or a horizontal tail. Before adding the icing effect, an analysis is performed to determine the relative distribution of lift and drag between the wing-fuselage and the horizontal tail. This analysis is performed using the 15,000 ft "day of" trim values. Starting with the relation for total airplane lift coefficient and solving for lift coefficient of the horizontal tail

$$\begin{aligned} C_L \bar{q}S &= C_{L_{\text{WF}}} \bar{q}S + C_{L_H} \bar{q}_H S_H \\ C_{L_H} &= \frac{C_L \bar{q}S - C_{L_{\text{WF}}} \bar{q}S}{\bar{q}_H S_H} = \frac{\bar{q}}{\bar{q}_H}\frac{S}{S_H}(C_L - C_{L_{\text{WF}}}) \\ &= \frac{1}{\eta}\frac{S}{S_H}(C_L - C_{L_{\text{WF}}}) \\ &= \frac{1}{0.945}\left(\frac{279.4}{70.04}\right)(0.377 - 0.359) = 0.073 \end{aligned} \tag{18}$$

To determine the lift coefficient of the wing-fuselage combination,

$$\begin{aligned} C_{L_{\text{WF}}} &= C_{L_{o_{\text{WF}}}} + C_{L_{\alpha_{\text{WF}}}}\alpha_W = C_{L_{o_{\text{WF}}}} + C_{L_{\alpha_{\text{WF}}}}(\alpha + i_W) = 0.034 \\ &+ 4.779(1.285 + 2.62)\frac{1}{57.3} = 0.034 + 0.3257 = 0.359 \end{aligned} \tag{19}$$

Table 2 Verification maneuver flight conditions and trim conditions

Altitude, ft	Airspeed, kn	Dynamic pressure, lb/ft^2	Weight, lb	Center of gravity, $\bar{c}$	α_1, deg	δ_1, deg
4631	101.9	30.1	7591	0.291	5.14	-0.572

Finally, the lift distribution between the horizontal tail and wing is determined using the ratio of Eqs. (18) and (19) to be

$$\frac{C_{L_H}}{C_{L_{\mathrm{WF}}}} = \frac{0.073}{0.359} = 0.203 \qquad C_{L_H} = 0.203 C_{L_{\mathrm{WF}}} \tag{20}$$

Thus, the horizontal tail generates approximately 20% of the lift that the wing-fuselage generates.

Although drag data were not available, drag data for a similar airplane configuration were used to provide a sanity check on the preceding lift ratio. Using $C_{D_{0_W}} = 0.37 C_{D_0}$ and $C_{D_{0_H}} = 0.07 C_{D_0}$,

$$C_{D_{0_H}} = \frac{0.07}{0.34} = 0.21 C_{D_{0_W}} \tag{21}$$

which confirms that the horizontal tail drag is also in the approximate proportion of 20% of the drag of the wing. Based on the values obtained in Eqs. (20) and (21), a 20% proportion is selected for the distributed icing condition. This proportion means that rather than calculating the dimensionalized derivative for the whole airplane and applying f_{ice} as in Eq. (16), each derivative is split into two components that are then added together using component buildup. This split allows for a separate icing factor to be applied to the lift and drag contribution of the wing and the lift and drag contribution of the horizontal tail.

V. Simulation Verification

To validate the mathematics and physics of the airplane model and simulation, a series of standard maneuvers were performed to determine if the airplane model responds correctly and consistently to control inputs for a conventional airplane configuration with conventional controls. The results are reported in [21], and show that the airplane model responds correctly to elevator and throttle inputs. Six verification maneuvers were performed and compared with flight test data to ensure that the simulation accurately represents a Cessna 208B Super Cargomaster. Flight test data were available for only a limited set of maneuvers, from which the verification maneuvers were selected. For brevity, only one of the verification maneuvers, response to an elevator singlet, is reproduced here.

Flight and trim conditions for the verification maneuver are shown in Table 2. The simulation and flight test airplane are both subjected to an elevator singlet to excite short period and phugoid responses. To ensure the greatest accuracy in comparing the simulation to flight test data, the elevator deflection history recorded from flight testing was used directly as the control input for the simulation. The time histories of the states, altitude, C_L, C_D, and elevator deflection for both the flight test data and the simulation are shown in Fig. 4. The airspeed responses of both the flight test airplane and the simulation are similar, with a maximum absolute airspeed difference at any given instant of time of 2.0%, where the absolute difference is defined as the maximum difference between the responses divided by the flight test data value at the instant of maximum difference. The

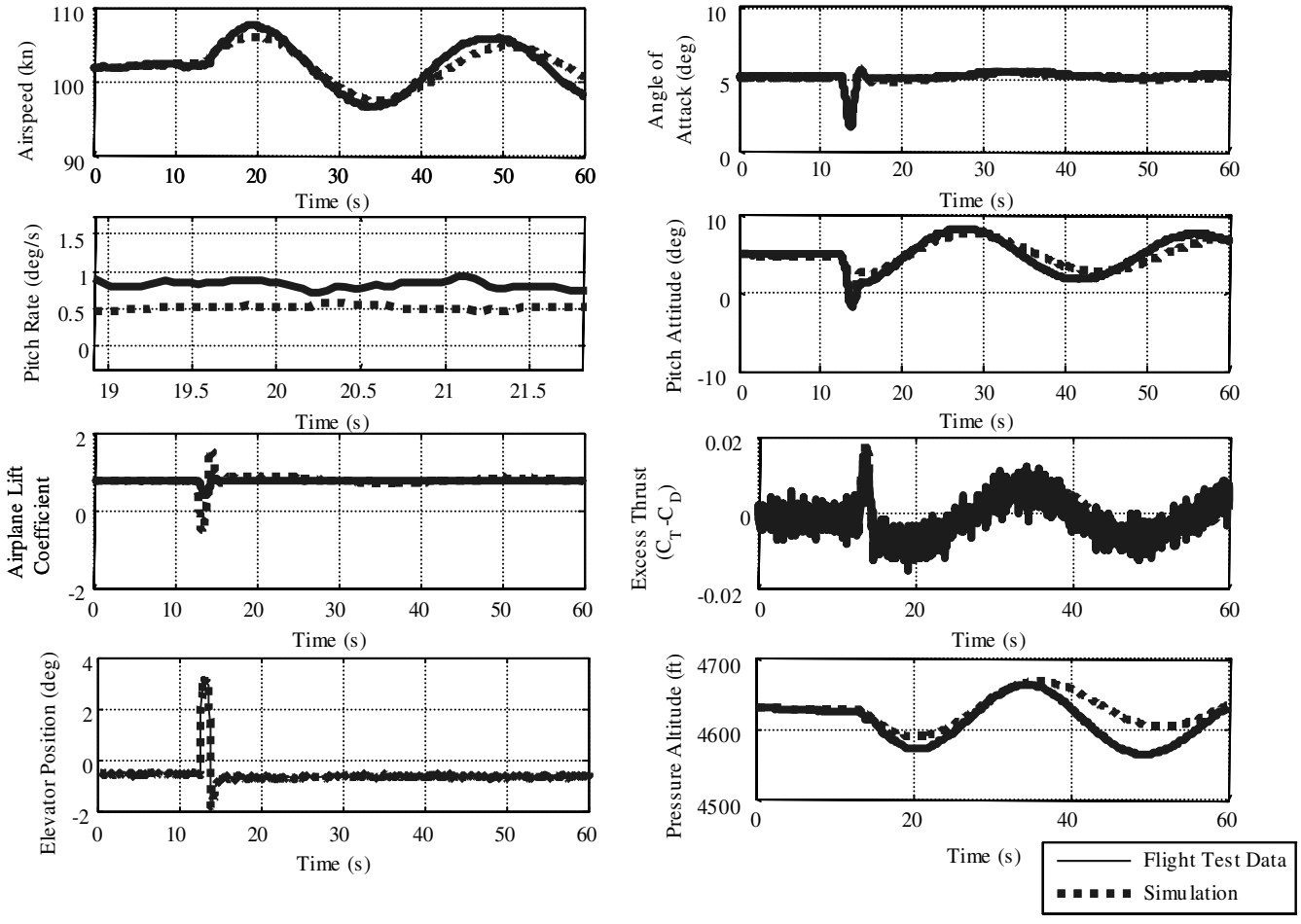

Fig. 4 Elevator singlet verification maneuver responses.

Table 3 Flight and trim conditions for cases 1–4

Altitude, ft	Airspeed, kn	Dynamic Pressure, lb/ft^2	Weight, lb	Center of gravity, $\bar{c}$	α_1, deg	δ_1, deg
15,000	113	30.55	8704	0.340	4.66	5.48

angle-of-attack responses also show similarities, with a maximum absolute difference of 3.0%. The error for the pitch rate appears high because the recorded flight test data do not provide a smooth time history and thus oscillates around the simulation time history. The nondimensionalized thrust minus airplane drag coefficient (row 3, column 2) has a constant offset of about 0.0175, because the value used for C_{D_0} was based on drag polars, not direct calculation. The simulation airplane lift coefficient, however, shows that the simulation is much more responsive to the elevator input than the flight test data suggests, but the response later in the time history is similar. Finally, the altitude time history again shows the similarity between the flight test data and the simulation. The difference is greatest at about 50 s into the simulation with an error of 1.0% between them.

Mismatches or errors noted in Fig. 4 between the flight test data and the simulation model arise from several sources. The first is that the simulation is an LTI model of a highly nonlinear time-variant system, and so small changes in the engine performance or control surface deflections are not accounted for in the model. Also, the model does not take into account external perturbations such as gusts that probably affected the flight test airplane to some extent during the test flights. In addition, it is only the short period response that truly matches well. There are differences in the phugoid frequency, damping ratio, and amplitude, though given the time frame in question to observe icing effects, phugoid mode discrepancies should not be an issue. Despite these inaccuracies, the response is generally as expected, and the longitudinal model is judged to be acceptable as an accurate representation of the airplane, within the limitations and accuracies of the methods used to construct the model.

VI. Simulation Examples

The simulation was used to evaluate several climb maneuvers for the purpose of determining the change in both dynamic response and performance due to various levels of ice accretion. Two test cases consisting of maximum power 2000 ft climbs under distributed icing (different levels of ice on the wing and horizontal tail) and a climb with an overly aggressive elevator input are presented to demonstrate the prediction of icing effects on airplane states and parameters such as altitude, airplane lift coefficient, and airplane drag coefficient. The data presented in Table 1 represent mixed icing conditions [6]. These are the degradation factors that are applied to the stability and control derivatives shown in Eq. (16), and they indicate how much the lift decreases, drag increases, and longitudinal stability decreases for each derivative. Subtracting each percentage from unity and applying it to the derivative indicated will effectively modify the airplane model for icing. In addition, an increase of 15% was applied to the total drag, based on data obtained for the Twin Otter that show an increase in drag of anywhere from 5 to ~30% [6,22]. For the purpose of direct comparison, weight and initial airspeed are the same for each case, shown in Table 3. For both the clean and iced airplane, airspeed is maintained at the recommended value of 113 kn to achieve the maximum rate of climb for the Cessna 208B [21].

A. Case 1: Climb from 15,000 to 17000 ft, Fully Iced Configuration

This case investigates a 2000 ft maximum power cruise climb from 15,000 to 17,000 ft over a period of 700 s, for a configuration with evenly distributed amounts of ice accretions on both the wing and horizontal tail. For this case, the full factors listed in Table 1 are applied to the model, representing an airplane fully accreted by ice. The ice accretions are known to alter the shape of the carefully engineered airfoil, thus decreasing its effectiveness at generating lift. Studies conducted at the University of Illinois on various airfoils with different types of ice accretions support this observation [5]. Also supported by these studies is an increase in drag caused by the ice accretions forming a horn or projection on the leading edge of the wing, thereby disrupting the airflow. This is shown in the airplane drag coefficient time history of Fig. 5, in which the drag is almost 320 counts greater for the iced case than the clean case. In terms of airplane drag, this count increase is very large. It is also important to note that the increase in angle of attack for the iced case was found to only contribute a small amount of induced drag to the total drag. The fully iced airplane has a trim angle of attack that is 5.34 or 0.7 deg greater than the clean airplane. The clean and iced airplanes both have initial climb rates of 210 and 160 ft/min, respectively, and then converge to the same decreased climb rate of less than 10 ft/min after 690 s. These initial differences in climb rate have an effect on achieved altitude, because the iced airplane can only climb to 15,940 ft, which is 310 ft less than the clean airplane even though airspeed is maintained close to the recommended 113 kn for a cruise climb [21]. The elevator time history indicates that the climb airspeed profile can only be maintained by flying very precisely, using only small elevator deflections. The sensitivity of the marginal rate of climb to very small elevator inputs is suggested by the maximum change in elevator deflection (0.2 deg as shown in Fig. 5) during this steady climb traversing less than the commanded 2000 ft altitude change. Figure 5 also demonstrates one of the major hazards of an iced airplane: it does not respond to pilot commands in the same manner as a clean airplane because the elevator deflection needed to maintain airspeed is dissimilar. This elevator sensitivity issue is investigated in detail in case 4. In total, the increased drag, increased climb attitude, and the necessity of a greater angle of attack for the fully iced configuration result in greatly reduced climb performance.

B. Case 2: Climb from 15,000 to 17000 ft, Distributed Icing Configuration

This case represents an airplane with distributed amounts of ice accreted on the wing and horizontal tail. The distribution of reduced lift and increased drag between the wing and horizontal tail according to Eqs. (18–21) is used for the simulation. Rather than just applying a universal percent of ice accretion accumulated on the lifting surfaces, different percentages are applied to the two lifting surfaces. In this case the wing is 70% iced and the horizontal tail is 40% iced. Relative to case 1, this distribution is considered moderate icing. The maneuver consists of a 2000 ft climb from 15,000 to 17,000 ft over a period of 700 s (Fig. 6). Airplane drag coefficient is increased by roughly 220 counts, which is not as great an increase as the fully iced case (case 1). The clean and iced airplanes each have initial climb rates of 210 and 180 ft/min, respectively, and then converge to the same decreased climb rate of less than 10 ft/min after 690 s. These initial differences in climb rate have an effect on achieved altitude because the iced airplane can only climb to 16,090 ft, which is 160 ft less than the clean airplane, even though airspeed is maintained close to the recommended 113 kn for a cruise climb [21]. As seen for case 1, the angle of attack needed to achieve the commanded altitude for an iced airplane is greater than for the clean airplane. Sensitivity of the marginal rate of climb to very small elevator inputs is exhibited, although elevator effectiveness is not compromised as much as in the fully iced case (case 1). The distributed icing configuration still requires a larger elevator deflection or a longer duration of elevator deflection to maintain airspeed in the attempt to achieve a 2000 ft commanded increase in altitude. These modified deflections introduce a greater likelihood for the flow over one or both of the lifting surfaces to separate.

C. Case 3: Climb from 15,000 to 17,000 ft, Fully Iced Configuration with Control Overshoot

This case represents an airplane fully accreted by ice subjected to aggressive pilot inputs, in this case an overshoot in elevator

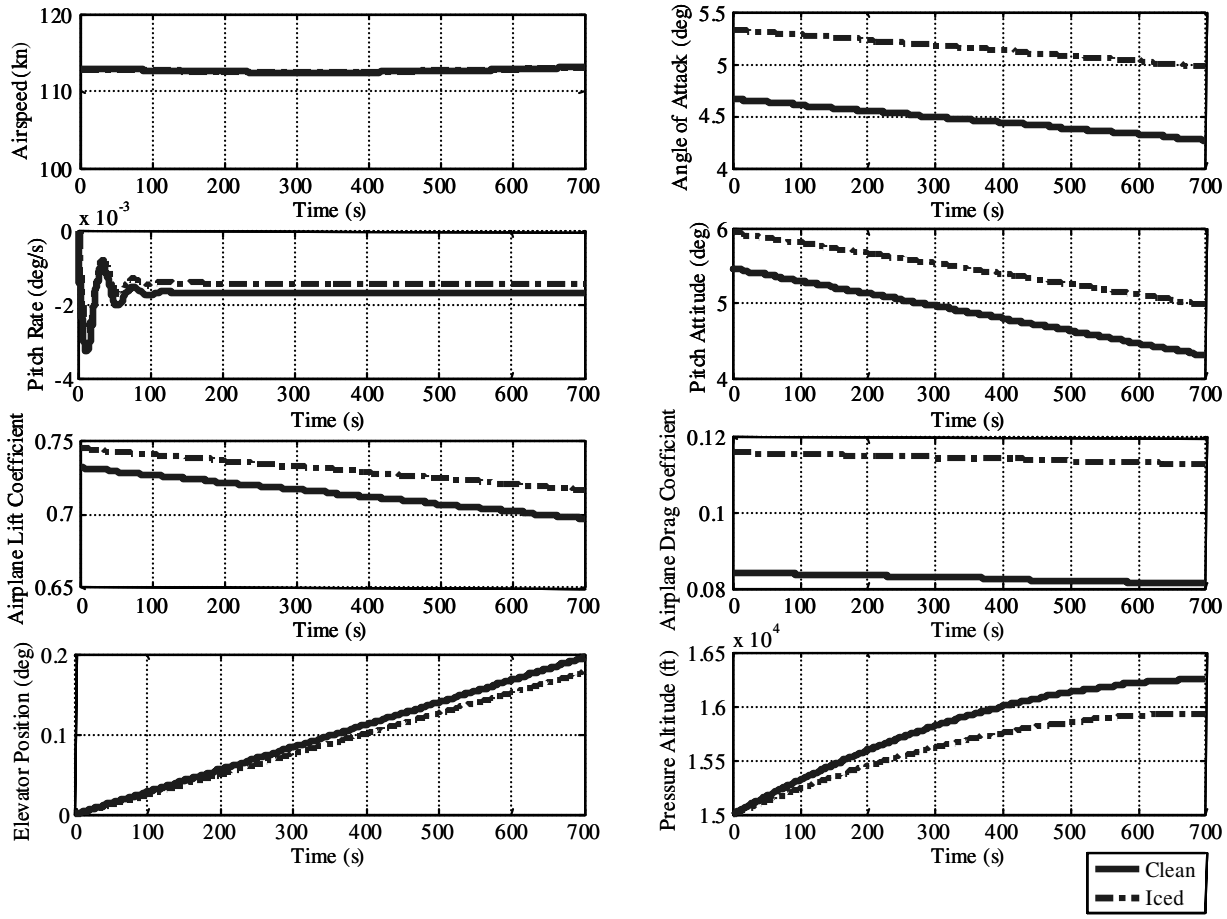

Fig. 5 Case 1: 2000 climb maneuver for clean and fully iced aircraft.

deflection of −1.5 deg for a period of 4 s introduced at the beginning of the climb. This important case simulates an overcorrection by the pilot as the airplane begins to climb, which can happen in situations when pilots are not aware of the severity of icing effects on the airplane. Only the first 100 s of the climb are of interest. Figure 7 shows the effects of overcontrolling a fully iced airplane and a clean airplane. The iced airplane begins the climb by responding with an excessive pitch attitude angle of 14.1 deg, and angle of attack is almost 50% greater than the trim angle of attack of 7.62 deg. As a result, airplane drag increases by an additional 200 counts above that for an already fully iced airplane that is subjected to nominal inputs. Furthermore, this peak in iced airplane drag is almost 500 counts above that for the nominal clean airplane before any control inputs. This example of overcorrection by the pilot during a climb with fully developed ice accretions demonstrates the increased potential for the flow over one or both lifting surfaces to separate, which can lead to departure from controlled flight. The clean airplane shows a similar response, although the angle of attack and peak drag are not nearly as large. These results highlight the sensitivity of an iced airplane response to pilot control inputs, and show the hazard of controlling an iced airplane as if it were clean. Although a pilot might safely overcontrol a clean airplane at the initiation of a climb, the results presented here show that doing so with the degraded aerodynamics and responses of an iced airplane is much more likely to lead to hazardous conditions, such as stall or departure from controlled flight.

VII. Conclusions

An analysis method using flight data, wind-tunnel data, and the U. S. Air Force Data Compendium was developed to create a basic but reasonably detailed and accurate simulation model that accounts for the dynamic effects of ice accretion on light airplanes. The component buildup method was used to implement icing effects on the wing alone, horizontal tail alone, and combined wing and horizontal tail using icing data on a similar light airplane. The icing data used were obtained empirically, and modified for the airplane configuration considered. The scope of the present work was limited to the pitch axis, where the most detrimental icing effects are typically experienced. A linear time invariant, state-space model of the longitudinal model of a representative light airplane was developed and used for non-real-time simulation to evaluate icing effects on stability and control characteristics, in addition to effects on performance such as climb maneuvers and descent maneuvers. Validation of the simulation model was conducted using several basic maneuvers, and verification was conducted using flight test data for the same airplane as the simulation. Numerical examples consisting of three attempted 2000 ft climbs in various levels of icing were evaluated, as well as an example consisting of an elevator singlet at the beginning of the climb. Based on the results presented in the paper, the following conclusions are drawn:

1) The linear state-space model representation, discrete simulation model, and inclusion of simplified icing effects appear to be an adequate tool for basic icing dynamics and performance analysis for the climb maneuver investigated. Comparing results to flight data showed good agreement for the long duration, gradual maneuvers investigated here, and only relatively simple data were needed to construct the models.

2) Qualitatively, from the simulation results, rate of climb and the ability to achieve commanded altitudes were seen to be sensitive to icing effects on elevator effectiveness, as compared with simulations maintaining the same recommended airspeeds for the same airplane in nonicing conditions. For all of the 2000 ft commanded climbs investigated, the iced airplane did not respond as quickly to elevator inputs as the clean airplane, due to decreased elevator effectiveness. Although larger elevator deflections or a longer duration of elevator

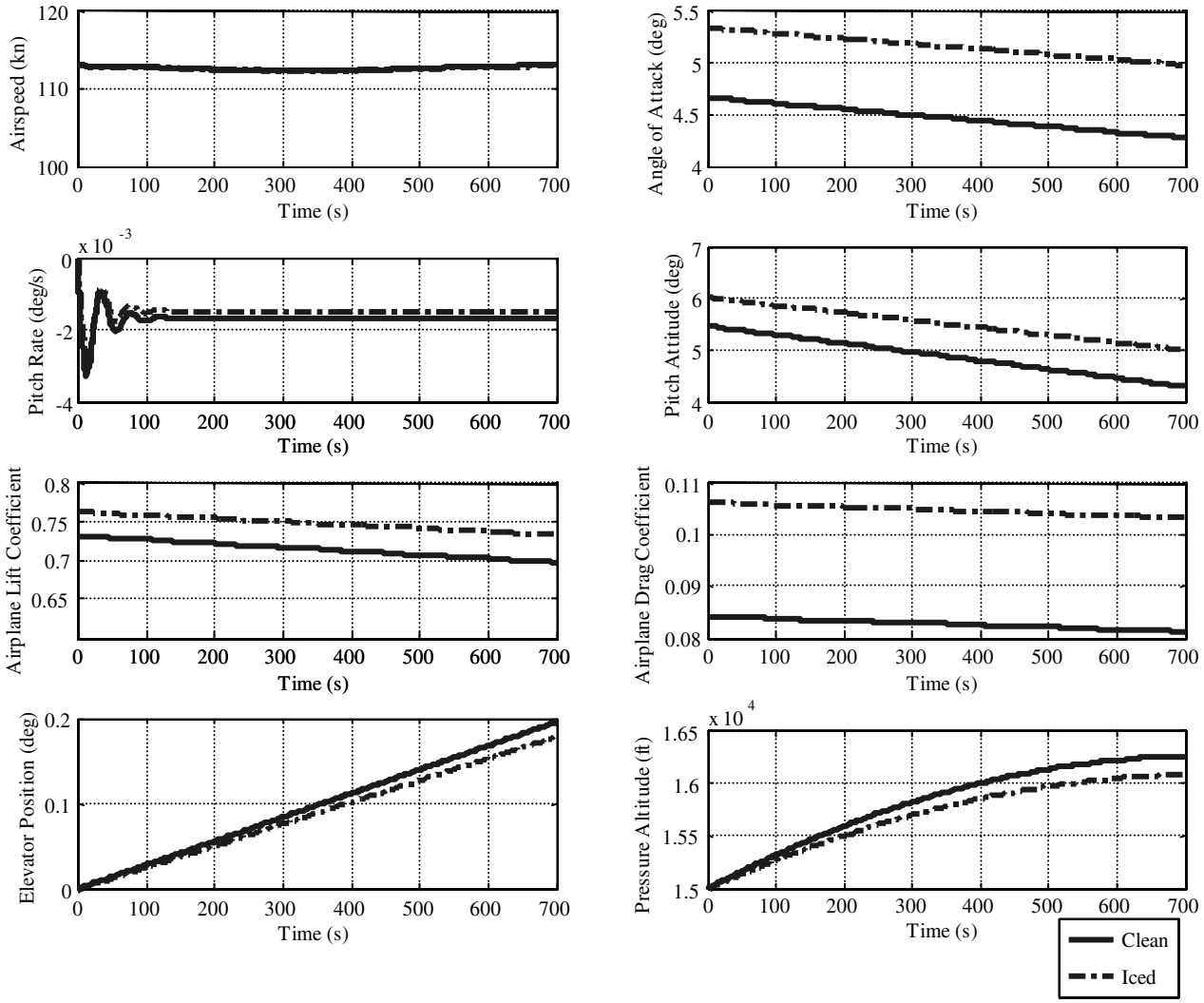

Fig. 6 Case 2: 2000 climb maneuver for clean and distributed iced aircraft.

input could be applied, doing so introduces a greater likelihood for the flow over one or both of the lifting surfaces to separate. The test case for a fully iced airplane with an aggressive elevator input further demonstrated the sensitivity to elevator deflection, in terms of excessive angle-of-attack and pitch attitude responses that could clearly induce a departure from controlled flight.

3) For the 2000 ft climb maneuver comparisons of the iced airplane to the clean airplane using the same elevator time histories, simulation results showed an adverse impact on climb performance:

a) The 100% iced configuration experienced a drag coefficient increase of 320 counts, which is a 300% increase compared with the 20% iced case. This configuration exhibited an angle-of-attack increase of 0.7 deg compared with the clean configuration.
   1) Rate of climb of the iced airplane was 50 ft/min less than that of the clean airplane.
   2) The iced airplane final altitude was 310 ft short of the clean airplane final altitude.

b) The distributed icing configuration (wing 70% iced, horizontal tail 40% iced) also suffered in climb performance. It exhibited a drag count increase of 220 counts as well as a 0.6 deg increase in angle of attack to maintain the climb, although overall climb performance was not as compromised as in the fully iced configuration.
   1) Rate of climb of the iced airplane was 30 ft/min less than that of the clean airplane.
   2) The iced airplane final altitude was 160 ft short of the clean airplane final altitude.

Appendix: Linear State-Space Models of Cessna 208 Super Cargomaster

Longitudinal dynamics (all angular quantities in radians):
Flight Condition: 101.92 kn, 4631 ft

$$\begin{bmatrix}\dot{u}\\ \dot{\alpha}\\ \dot{q}\\ \dot{\theta}\end{bmatrix}=\begin{bmatrix}-0.05 & 17.44 & 0 & -32.05\\ -0.0021 & -1.14 & 0.96 & -0.016\\ -0.0031 & -6.81 & -1.83 & 0.0018\\ 0 & 0 & 1 & 0\end{bmatrix}\begin{bmatrix}u\\ \alpha\\ q\\ \theta\end{bmatrix}+\begin{bmatrix}-0.42 & 2.79\\ -0.11 & 0\\ -6.86 & 0\\ 0 & 0\end{bmatrix}\begin{bmatrix}\delta_e\\ \delta_T\end{bmatrix}$$

Flight Condition: 135 kn, 15,000 ft

$$\begin{bmatrix}\dot{u}\\ \dot{\alpha}\\ \dot{q}\\ \dot{\theta}\end{bmatrix}=\begin{bmatrix}-0.03 & 17.74 & 0 & -32.17\\ -0.0013 & -1.17 & 0.97 & -0.0031\\ -0.0005 & -8.71 & -1.79 & 0.0003\\ 0 & 0 & 1 & 0\end{bmatrix}\begin{bmatrix}u\\ \alpha\\ q\\ \theta\end{bmatrix}+\begin{bmatrix}-0.55 & 2.79\\ -0.11 & 0\\ -8.78 & 0\\ 0 & 0\end{bmatrix}\begin{bmatrix}\delta_e\\ \delta_T\end{bmatrix}$$

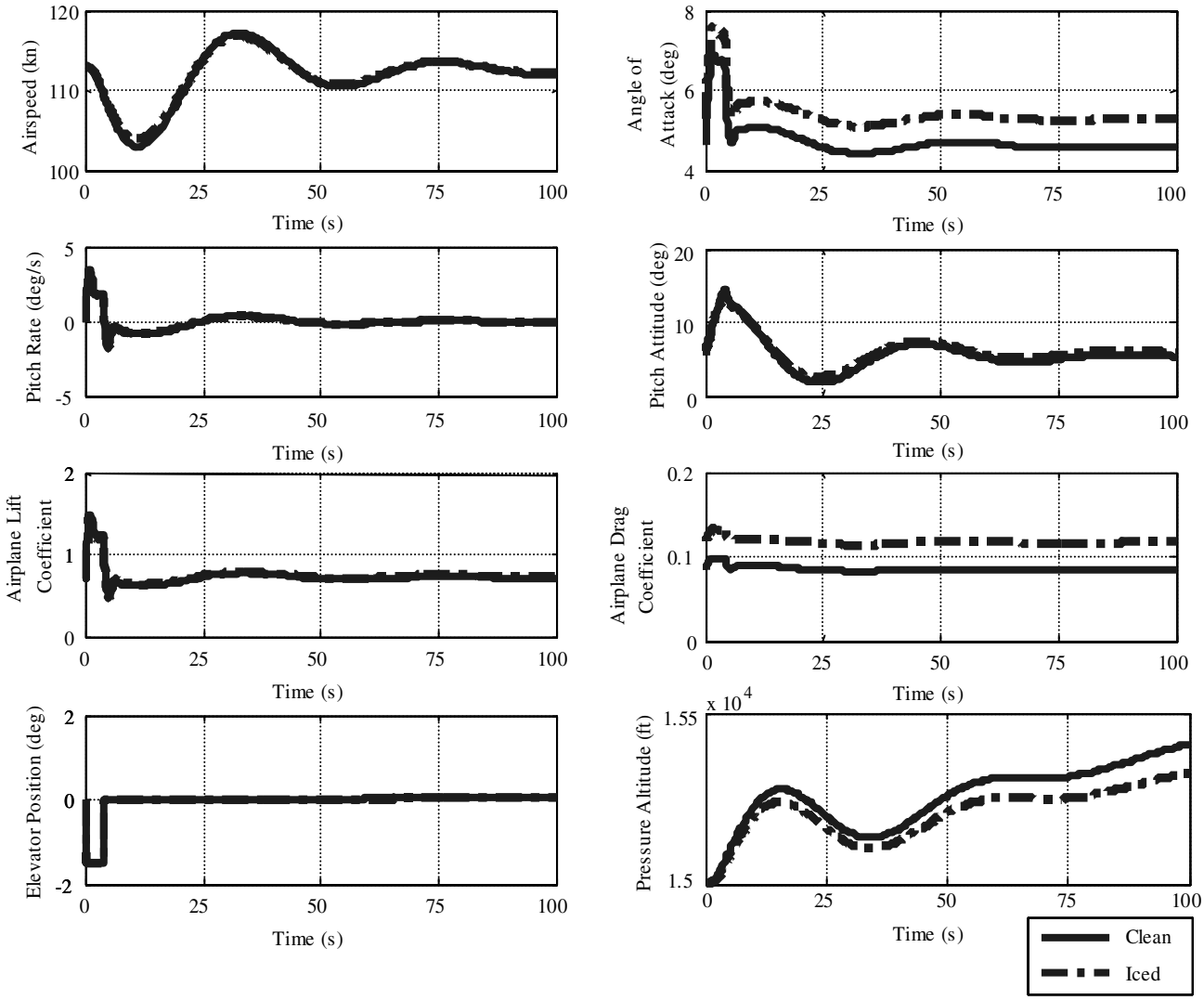

Fig. 7 Case 3: climb from 15,000 to 17,000 ft, fully iced configuration with control overshoot.

Acknowledgments

This research is funded by the Aeronautical and Educational Services Company, under grant number C05-00356. The technical monitor is Donald T. Ward. Propulsion data and flight data for the simulation model were provided by Kohlman Systems Research, Inc. The authors gratefully acknowledge all of this support. The authors also wish to thank the reviewers for their many comments and suggestions which have improved the paper.

References

[1] Anon., "Annual Review of Aircraft Accident Data: U.S. General Aviation, Calendar Year 1998," National Transportation Safety Board, Washington, DC, 2003, pp. 35, 39.

[2] Anon., "Annual Review of Aircraft Accident Data: U.S. General Aviation, Calendar Year 1999," National Transportation Safety Board, Washington, DC, 2003, pp. 32, 39.

[3] Anon., "Annual Review of Aircraft Accident Data: U.S. General Aviation, Calendar Year 2000," National Transportation Safety Board, Washington, DC, 2004, pp. 38, 41.

[4] Anon., "Annual Review of Aircraft Accident Data: U.S. General Aviation, Calendar Year 1997," National Transportation Safety Board, Washington, DC, 2004, pp. 38, 41.

[5] Gurbacki, H. M., and Bragg, M. B., "Unsteady Aerodynamic Measurements on an Iced Airfoil," AIAA Paper 2002-0241, Jan. 2002.

[6] Bragg, M. B., Hutchison, T., Merret, J., Oltman, R., and Pokhariyal, D., "Effect of Ice Accretion on Aircraft Flight Dynamics," AIAA Paper 2000-0360, Jan. 2000.

[7] Rauw, M., "FDC 1.3," SIMULINK Toolbox for Flight Dynamics and Control Analysis, 1998, available at http://www.mathworks.com/matlabcentral/fileexchange.

[8] Sharma, V., Voulgaris, P. G., and Frazzoli, E., "Aircraft Autopilot Analysis and Envelope Protection for Operation Under Icing Conditions," *Journal of Guidance, Control, and Dynamics*, Vol. 27, No. 3, 2004, pp. 454–465.

[9] Sibilski, K., Lasek, M., Ladyzynska-Kozdras, E., and Maryniak, J., "Aircraft Climbing Flight Dynamics With Simulated Ice Accretion," AIAA Paper 2004-4948, Aug. 2004.

[10] Lee, S., and Bragg, M. B., "Experimental Investigation of Simulated Large-Droplet Ice Shapes on Airfoil Aerodynamics," *Journal of Aircraft*, Vol. 36, No. 5, 1999, pp. 844–850.

[11] Broeren, A. P., Addy, H. E., Jr., and Bragg, M. B., "Effect of Intercycle Ice Accretions on Airfoil Performance," *Journal of Aircraft*, Vol. 41, No. 1, 2004, pp. 165–174; also AIAA Paper 2002-0240, Jan. 2002.

[12] Whalen, E., and Bragg, M., "Aircraft Characterization in Icing Using Flight-Test Data," *Journal of Aircraft*, Vol. 42, No. 3, 2005, pp. 792–794.

[13] Broeren, A. P., and Bragg, M. B., "Effect of Airfoil Geometry on Performance with Simulated Intercycle Ice Accretions," *Journal of Aircraft*, Vol. 42, No. 1, 2005, pp. 121–130; also AIAA Paper 2003-0728, Jan. 2003.

[14] Bragg, M. B., "Aircraft Aerodynamic Effects Due to Large Droplet Ice Accretions," AIAA Paper 96-0932, Jan. 1996.

[15] Lu, B., and Bragg, M. B., "Airfoil Drag Measurement with Simulated Leading-Edge Ice Using the Wake Survey Method," AIAA Paper 2003-1094, Jan. 2003.

[16] Broeren, A. P., Addy, H. E., Jr., and Bragg, M. B., "Flowfield Measurements About an Airfoil with Leading-Edge Ice Shapes," AIAA

Paper 2004-0559, 2004.
[17] Bragg, M. B., Perkins, W. R., Sarter, N. B., Basar, T., Voulgaris, P. G., Gurbacki, H. M., Melody, J. W., and McCray, S. A., "Interdisciplinary Approach to Inflight Aircraft Icing Safety," AIAA Paper 98-0095, Jan. 1998.
[18] Bragg, M. B., Basar, T., Perkins, W. R., Selig, M. S., Voulgaris, P. G., Melody, J. W., and Sarter, N. B., "Smart Icing Systems for Aircraft Icing Safety," AIAA Paper 2002-0813, Jan. 2002.
[19] Anon., "Advanced Aircraft Analysis," Design, Analysis, and Research Corp., Lawrence, KS, 2003.
[20] Anon., "Cessna Aircraft Company Model 208 Maintenance Manual," Cessna Aircraft Co., Wichita, KS, April 1996.
[21] Lampton, A., and Valasek, J., "Prediction of Icing Effects on the Stability and Control of Light Airplanes," *Proceedings of the AIAA Atmospheric Flight Mechanics Conference, San Francisco, CA*, AIAA Paper 2005-6219, 2005.
[22] Bragg, M. B., and Lee, S., "Aircraft Icing Flight Dynamics Model for Twin Otter Aircraft," Final Technical Rept. 10817/1329/TTM to Systems Technology, Hawthorne, CA, 4 Oct. 2000.